Journal of Power Sources 213 (2012) 160–168

Contents lists available at SciVerse ScienceDirect

Journal of Power Sources

journal homepage: www.elsevier.com/locate/jpowsour

Effects of cell positive cans and separators on the performance of high-voltage Li-ion batteries

Xilin Chen [a], Wu Xu [a,*], Jie Xiao [a], Mark H. Engelhard [a], Fei Ding [a,b], Donghai Mei [a], Dehong Hu [a], Jian Zhang [a], Ji-Guang Zhang [a,**]

[a] Pacific Northwest National Laboratory, Richland, WA 99354, USA
[b] National Key Laboratory of Power Sources, Tianjin Institute of Power Sources, Tianjin 300381, PR China

ARTICLE INFO

Article history:
Received 25 February 2012
Received in revised form
31 March 2012
Accepted 2 April 2012
Available online 24 April 2012

Keywords:
Lithium-ion battery
High-voltage cathode
Positive can
Separator
Efficiency
Cycling stability

ABSTRACT

The effects of different cell positive cans and separators on first-cycle Coulombic efficiency and long-term cycling stability of a high-voltage spinel cathode are investigated systematically. Compared to stainless steel (SS) positive cans, aluminum (Al)-clad SS-316 positive cans are much more resistant to oxidation at high voltages; therefore, the initial Coulombic efficiency of the batteries with Al-clad can is improved by more than 13%. Among the five separators studied in this work, the polyethylene (PE) separator exhibits the best electrochemical stability. The cells using $LiCr_{0.05}Ni_{0.45}Mn_{1.5}O_4$ as the cathode, an Al-clad positive can, and a PE separator exhibits a first-cycle Coulombic efficiency of about 90% and a capacity fading of only 0.01% per cycle.

1. Introduction

The energy densities and cycling stabilities of state-of-the-art lithium (Li)-ion batteries still are not sufficient to meet requirements set by the U.S. Department of Energy for electric vehicles [1–4]. Significant efforts have been made worldwide to increase the energy densities of Li-ion batteries by employing cathode materials with higher specific capacities and/or higher operating voltages. High-voltage spinel cathode materials, such as $LiNi_{0.5}Mn_{1.5}O_4$ and its doped analogs [5–11], have a flat voltage profile of about 4.75 V vs. Li/Li^+ and a theoretical specific energy of about 650 Wh kg^{-1}, which are 20% and 30% higher than those of conventional $LiCoO_2$ and $LiFePO_4$ materials [12], respectively. However, the first-cycle efficiencies of high-voltage spinel cathode materials reported in literature are relatively low, only in the range of 75 ~ 84% [6,8,9,13]. For example, an initial efficiency of 75% was reported for $LiNi_{0.5}Mn_{1.5}O_4$ spinel by Shaju and Bruce [6], and for $LiNi_{0.5}Mn_{1.2}Ti_{0.3}O_4$ by Liu et al. [8]. Sun et al. [9] and Zhang et al. [13] obtained slightly higher first-cycle efficiencies for $LiNi_{0.5}Mn_{1.5}O_4$ (80.6% and 83.6%, respectively). However, the reasons for these low initial Coulombic efficiencies are not well understood.

In our early studies on high-voltage cathode materials such as Li_2CoPO_4F [14] and $LiNi_{0.5}Mn_{1.5}O_4$ [15], we found that the non-electrochemically active materials significantly affect the performances of the high-voltage cathode materials. These non-active materials include the positive cans of coin cells, separators, and electrolytes. Very recently, Dahn and coworkers [16] reported that the corrosion of SS hardware for coin cells at high potentials may affect the performance evaluation of the high-voltage cathode materials. Localized corrosion observed when the cells were charged to 4.6 V was attributed to the existence of hydrogen fluoride (HF) in the non-aqueous electrolyte. However, Dahn and coworkers used positive cans (without active cathode) as the working electrodes in their study and did not report the effect of the positive can on the performance of cathode materials. In this work, we systematically investigated the effects of positive cans and separators on cell performance, especially on the first-cycle efficiency and long-term cycling stability of a 5% chromium (Cr)-doped $LiNi_{0.5}Mn_{1.5}O_4$ material (i.e., $LiCr_{0.05}Ni_{0.45}Mn_{1.5}O_4$). The results obtained from our work also can be applied to the selection

* Corresponding author. Tel.: +1 509 375 6934; fax: +1 509 375 3864.
** Corresponding author. Tel.: +1 509 372 6515; fax: +1 509 375 3864.
E-mail addresses: wu.xu@pnnl.gov (W. Xu), jiguang.zhang@pnnl.gov (J.-G. Zhang).

0378-7753/$ – see front matter © 2012 Elsevier B.V. All rights reserved.
doi:10.1016/j.jpowsour.2012.04.009

of appropriate active and non-active materials used in other high-voltage battery systems.

2. Experimental

In this study, CR2032 type coin cell kits (including positive cans, negative covers, spacers, and springs all made of SS-316, Al-clad SS-316 positive cans, and polypropylene [PP] gaskets) were purchased from MTI Corporation. The separators were supplied by Celgard, including Celgard K1640 monolayer PE membrane, Celgard 2500 monolayer PP membrane, Celgard 2325 trilayer PP/PE/PP membrane, and Celgard 3501 surface-modified PP membrane. A polyvinylidene fluoride (PVDF) separator also was investigated and compared with polyolefin separators. The PVDF separator was prepared by coating a thin PVDF layer onto the Celgard 2500 PP membrane. In the coating process, the Celgard 2500 separator was immersed in a 1% PVDF/acetone solution for 1 min, removed from the solution to allow the acetone to evaporate, and then dried in a vacuum oven for several hours.

The high-voltage cathode material $LiCr_{0.05}Ni_{0.45}Mn_{1.5}O_4$ was synthesized by ball milling a mixture of Li_2CO_3, NiO, Cr_2O_3, and $MnCO_3$ (all from Sigma–Aldrich) in stoichiometric amounts for 4 h. The milled material was heat treated at 900 °C for 24 h in air and further annealed at 700 °C for 8 h. The synthesis process and characterization of this material were reported elsewhere [15]. The cathode sheet was prepared by casting a slurry of $LiCr_{0.05}Ni_{0.45}Mn_{1.5}O_4$, super P (SP, from Timcal), and PVDF (Kynar HSV900, from Arkema Inc.) in an *N*-methyl pyrrolidone (Aldrich) solvent onto Al foil (from All Foils, Inc.). The weight ratio of $LiCr_{0.05}Ni_{0.45}Mn_{1.5}O_4$:SP:PVDF was 80:10:10. After the solvent was evaporated, the cathode sheet was pressed at 3000 psi for 1 min. Disks with a diameter of 1.27 cm were die cut and dried overnight under vacuum at 110 °C.

Half cells were assembled in an argon-filled MBraun glove box using Li metal as the anode and 1-M $LiPF_6$ in EC/EMC (3:7 ratio in volume) as the electrolyte. The electrochemical performance of the coin cells was measured at room temperature using an Arbin BT-2000 battery tester (Arbin Instruments). The cells were cycled between 3.0 and 4.9 V. Cyclic voltammetry (CV) scans were conducted on a CHI 1000A impedance analyzer (CH Instruments) at a scan rate of 0.01 mV s^{-1} measured between 3.0 and 4.9 V using a two-electrode cell configuration. The positive cans and separators from cycled coin cells were analyzed by X-ray photoelectron spectroscopy (XPS) with a Physical Electronics Quantera Scanning X-Ray Microprobe. The samples were obtained from disassembled cells, washed three times with anhydrous EMC, dried in the antechamber of the glove box under vacuum, and mounted onto the standard Physical Electronics 75 mm × 75 mm sample holder using 2-56 stainless steel screws inside a nitrogen re-circulated glove box operated at <0.2 ppm oxygen and a dew point of 80 °C. The XPS system used a focused monochromatic Al Kα X-ray (1486.7 eV) source for excitation and a spherical section analyzer. A 200-μm diameter focused X-ray spot was used for the analysis. The separators from cycled coin cells were also analyzed by FTIR (Bruker Optics Vertex 70 FTIR) in transmission mode with a resolution of 4 cm^{-1}. The separators were directly mounted on the holders and no other objects were in the IR beam. % transmission was calculated using air as reference. Density functional theory (DFT) method was used to calculate highest occupied molecular orbital (HOMO) and the lowest unoccupied molecular orbital (LUMO) energies of model polymer (PE, PP, and PVDF) materials to study the electrochemical stability of PP, PE and PVDF. The morphology of the surface and cross-section of Celgard 2500 and PVDF-coated Celgard 2500 separators was observed by scanning electron microscopy (JSM-5900 Jeol).

3. Results and discussion

3.1. Effect of cell positive cans

Fig. 1 compares the CV curves of the coin cells using two different positive cans made of SS-316 and Al-clad SS-316. In all these cells, Celgard K1640 PE separators were used. The small broad redox peaks at ~4.0 V for both cells are associated with the Mn^{3+}/Mn^{4+} redox couple, and the two large sharp redox peaks at ~4.7 V are attributed to the Ni^{2+}/Ni^{4+} redox couple of the $LiCr_{0.05}Ni_{0.45}Mn_{1.5}O_4$ cathode [6,17–23].

The first- and second-cycle CV curves for the SS-316 positive cans show large differences for the two pairs of redox peaks ascribed to Ni^{2+}/Ni^{4+} (at ~4.7 V; Fig. 1(a)). These differences mainly result from oxidation of the SS-316 positive can when the cell is charged over 4.5 V. As reported by Dahn and coworkers [16], some metal oxides such as Fe_2O_3 and Cr_2O_3 always exist on the surface of commercial coin cell cans made of SS-316. On the other hand, $LiPF_6$-based electrolytes always contain trace amount of HF and other acidic species generated by the reactions of $LiPF_6$ with residual water in electrolyte and electrodes. The protective layers of Fe_2O_3 and Cr_2O_3 may be corroded by the acidic species at high voltages, and chromium (Cr) and iron (Fe) ions may dissolve into the electrolyte [16]. Then, the inner Fe and other metal elements in the can made of SS-316 will be exposed to the electrolyte and oxidized during subsequent charge processes. When comparing the XPS results of the SS-316 can before and after battery testing (shown in Fig. 2(a)), more and higher intensity iron peaks appear on the surface of the SS-316 positive can after cycling, which supports the explanation stated above. The deposited elements of fluorine (F) and phosphorus (P) are from decomposition of the lithium salt $LiPF_6$.

However, when an Al-clad SS-316 positive can is used, the CV curves in the first two cycles are almost identical (Fig. 1(b)) because a thin, but dense, alumina layer exists on the surface of the cans. This alumina protection layer does not break down at high voltages (~4.9 V) and can protect the inner SS-316 materials from corrosion by HF and other acidic species when the cell is charged to more than 4.5 V. This finding is consistent with the XPS results shown in Fig. 2(b). After cycling, only limited intensity changes are observed

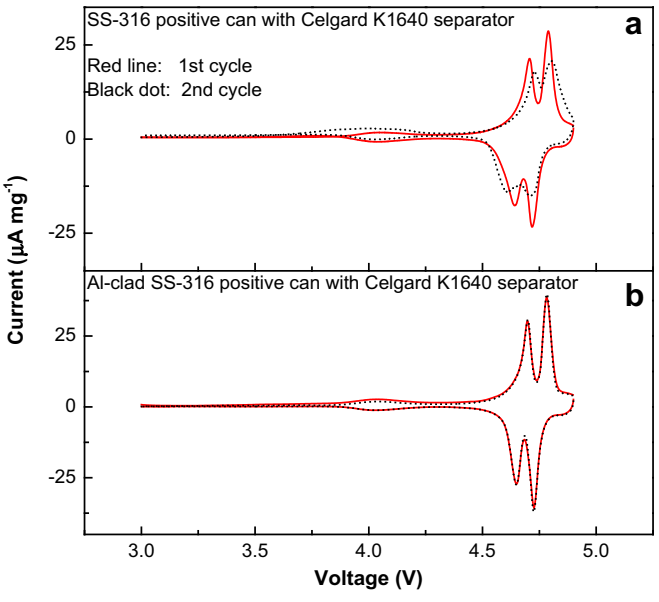

Fig. 1. CV scan curves of Li/$LiCr_{0.05}Ni_{0.45}Mn_{1.5}O_4$ half cells using a) an SS-316 positive can and b) an Al-clad SS-316 positive can, with a Celgard K1640 PE separator.

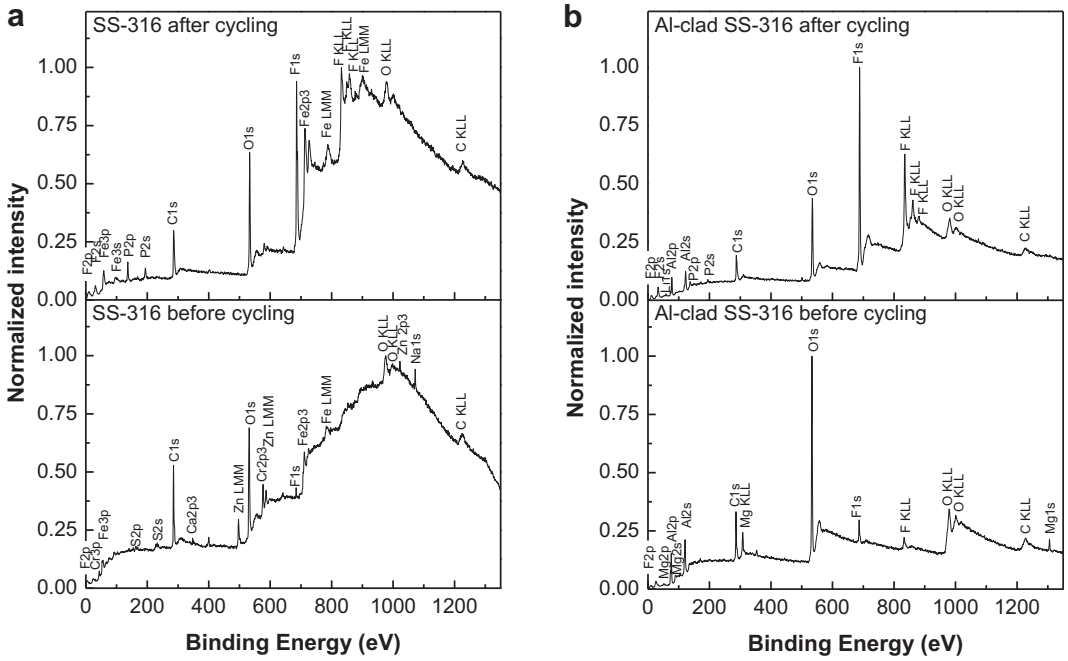

Fig. 2. XPS spectra of a) an SS-316 positive can and b) an Al-clad SS-316 positive can before and after cycling in Li/LiCr$_{0.05}$Ni$_{0.45}$Mn$_{1.5}$O$_4$ half cells.

for the elements from the XPS spectra measured on the surface of Al-clad cans – that is, the decrease in intensity for oxygen (O), Al, and magnesium (Mg), the increase in intensity for F, and the appearance of P and Li, all of which result from depositions of decomposed electrolyte salt and solvents, but not from the SS-316 cans.

Fig. 3 compares the voltage profiles from the first two charge and discharge processes of the Li/LiCr$_{0.05}$Ni$_{0.45}$Mn$_{1.5}$O$_4$ half cells using two different positive cans with Celgard K1640 PE separators. Three clear plateaus appear at about 4.05, 4.70, and 4.78 V during the charge process, and corresponding plateaus at 4.00, 4.65, and 4.72 V during the discharge process also are observed, which is consistent with the CV results shown in Fig. 1. During the charge process, the cell using the SS-316 positive can has a broader plateau between 4.70 and 4.78 V than the cell using the Al-clad SS-316 can. This result suggests that oxidation of the SS-316 positive cans co-exists with the oxidation of Ni^{2+} in the cathode material. The Coulombic efficiencies of the Li/LiCr$_{0.05}$Ni$_{0.45}$Mn$_{1.5}$O$_4$ cell using the SS-316 can are only 76.4% and 83.0% in the first and second cycles, respectively. However, when using the Al-clad SS-316 can, these efficiencies can reach 89.6% and 95.5%, respectively. In addition to the formation of a cathode surface film in the first cycle, the increased irreversible charge capacity for the cell can be attributed to oxidation of the SS-316 can at high voltages. This result demonstrates that Al-clad SS positive cans are much more stable against oxidation at high voltages.

The rate performance and long-term cycling stability of the Li/LiCr$_{0.05}$Ni$_{0.45}$Mn$_{1.5}$O$_4$ half cells using SS-316 and Al-clad SS-316 positive cans are shown in Fig. 4. Celgard K1640 PE separators were used in these cells. The test program combined various-rate cycling

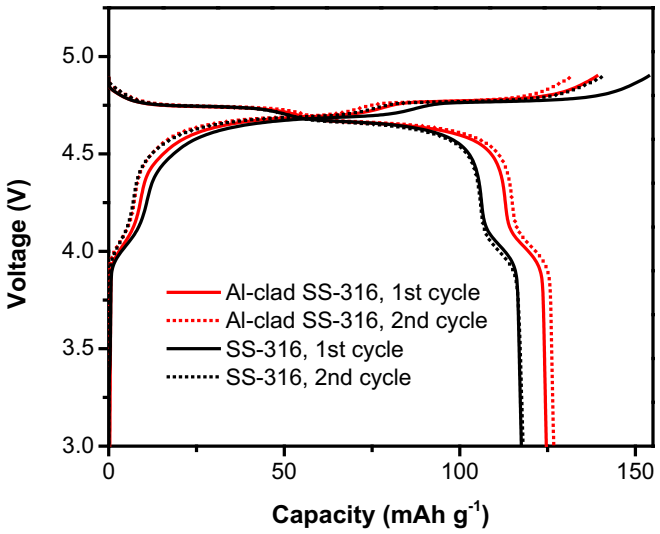

Fig. 3. Voltage profiles of the first two charge-discharge processes of Li/LiCr$_{0.05}$Ni$_{0.45}$Mn$_{1.5}$O$_4$ half cells using an SS-316 can and an Al-clad SS-316 can, with a Celgard K1640 PE separator.

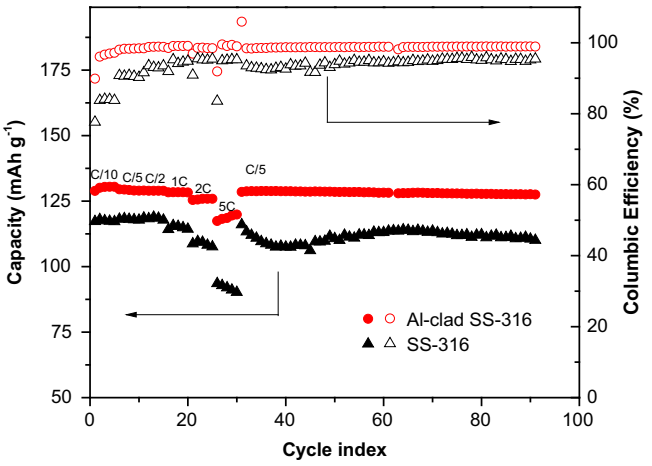

Fig. 4. Rate performance, long-term cycling stability, and Coulombic efficiency of Li/LiCr$_{0.05}$Ni$_{0.45}$Mn$_{1.5}$O$_4$ half cells using an SS-316 can and an Al-clad SS-316 can, with a Celgard K1640 PE separator.

and long-term cycling. In the rate cycling performance test, the charge rate was C/10 for the first five cycles and C/5 for all other cycles, while discharge rates between C/10 and 5C were used in the first 30 cycles, and each rate was set for 5 cycles. Following the rate performance test, the long-term cycling stability was tested at a C/5 rate for both the charge and discharge processes. Fig. 4 clearly demonstrates that the cell using the Al-clad SS-316 can has higher specific capacities, much better rate performance, and longer cycling stability than the cell using the SS-316 can. In addition, the Coulombic efficiency of the cell using the Al-clad SS-316 can reaches 99.1% after only five cycles and stays stable, but the Coulombic efficiency of the cell using the SS-316 can shows poor cycling efficiency, fluctuating between 90.3% and 95.9% after five cycles. The significant improvement in capacity, cycling efficiency, rate capability, and stability clearly shows that the SS-316 cans typically used in low-voltage Li-ion batteries should be replaced by the Al-clad SS-316 cans when a high-voltage cathode (such as $LiNi_{0.5}Mn_{1.5}O_4$ spinel) is used.

3.2. Effect of separators

Because most commercially available separators have been used extensively in Li-ion batteries with voltages less than 4.5 V, their stabilities at higher voltages (e.g., 5 V) need to be examined before they are used in high voltage Li-ion batteries. Fig. 5 shows the CV curves of the $Li/LiCr_{0.05}Ni_{0.45}Mn_{1.5}O_4$ half cells using Al-clad SS-316 positive cans and five different separators including 1) Celgard K1640, 2) Celgard 2325, 3) Celgard 2500, 4) Celgard 3501, and 5) PVDF-coated Celgard 2500. As shown in Fig. 5, the CV curves from the first two scans are almost identical for cells using Celgard K1640 PE separators, have slight difference for the cells with Celgard 2325 PP/PE/PP and PVDF-coated Celgard 2500 separators, but show significant difference for the cells with Celgard 3501 and Celgard 2500 separators. Among the five separators, only Celgard 3501 (a surface-modified PP membrane with certain surfactants) shows a small but broad oxidation peak, with a spike at about 4.6 V during the first anodic scan. The two peaks can be attributed to oxidation of the coating materials as shown by XPS analysis and discussed in the next section of this paper. For the cells using Celgard 3501 and Celgard 2500 separators, the current density of the anodic scan during the first scan is higher than that in the second scan at voltages greater than 4.3 V. This change in current density likely results from the reactions (i.e., passivation) among the active materials, the separator and the electrolyte when the cells are charged to higher voltages. The variation between the first and second CV scans for the Celgard 2500 PP separator can be greatly suppressed by coating a layer of PVDF as shown in Fig. 5(e), thus verifying that the variation between the first and second CV scans at high voltages results from reactions that occurred on the separator surface.

Fig. 6 shows the rate capability and long-term cycling stability of the $Li/LiCr_{0.05}Ni_{0.45}Mn_{1.5}O_4$ half cells using Al-clad SS-316 coin cell cans and various separators, including Celgard K1640, Celgard 2325, Celgard 2500, Celgard 3501, and PVDF-coated Celgard 2500. The Columbic efficiencies of the first charge/discharge cycle are in the order of 66.4 ± 1.3% for Celgard 3501 <82.2 ± 4.1% for Celgard 2500 <84.9 ± 5.3% for Celgard 2325 <86.3 ± 0.1% for PVDF-coated Celgard 2500 <89.6 ± 2.4% for Celgard K1640. The capacity retention at low C-rates (i.e. C/10, C/5, C/2 and 1C) has the same trend (Celgard 3501 < Celgard 2500 < Celgard 2325 < PVDF-coated Celgard 2500 < Celgard K1640). Higher initial irreversible capacity corresponds to lower capacity retention. It corroborates that there is a little active material loss in the initial cycle due to the aforementioned reactions among the active material, electrolyte and separators. Among the cells with the five separators, the cell with the Celgard 3501 separator exhibits the lowest first-cycle Columbic efficiency, the lowest capacity at low rates, and the second poorest high-rate performance. The main reason for this poor performance is the instability of the surface-coated surfactant at high voltages. The cell with the Celgard K1640 PE separator shows the highest first-cycle efficiency, which also is much higher than the results reported in literature [6,8,9,13], and also the highest capacity, high-rate capability, and long-term cycling stability. This result demonstrates that PE is very stable at high voltages. The cell with the Celgard 2500 separator, which is PP, exhibits low capacity, fast capacity fading, and the poorest high-rate performance. Its performance is even worse than the cells with Celgard 3501 separator when the current rate is over 2C, which indicates that PP is not stable at high voltages. In terms of first-cycle efficiency, capacity, cycling stability, and rate capacity, the cells with a Celgard

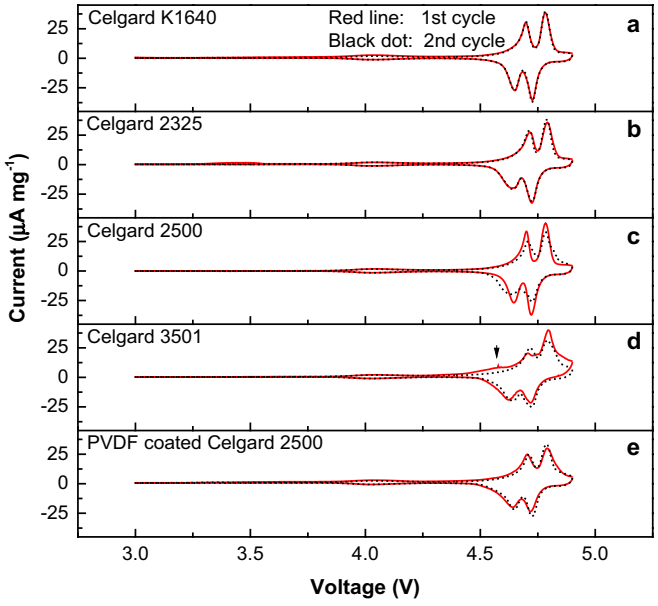

Fig. 5. CV curves of $Li/LiCr_{0.05}Ni_{0.45}Mn_{1.5}O_4$ half cells using Al-clad SS-316 coin cell cans and various separators, including a) Celgard K1640, b) Celgard 2325, c) Celgard 2500, d) Celgard 3501, and e) PVDF-coated Celgard 2500.

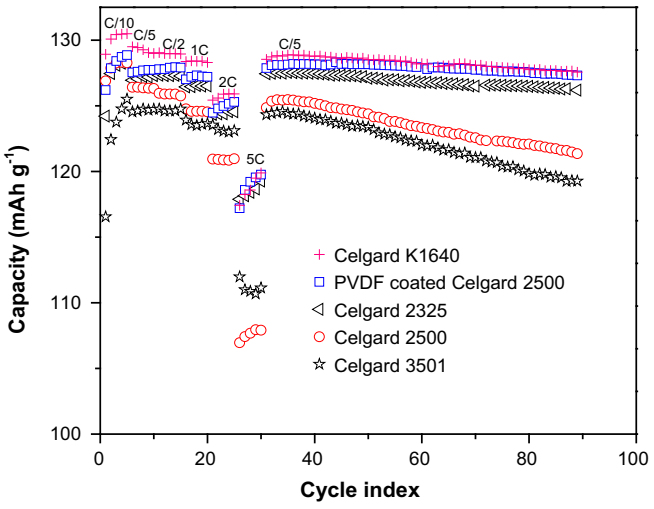

Fig. 6. Rate performance and long-term cycling stability of $Li/LiCr_{0.05}Ni_{0.45}Mn_{1.5}O_4$ half cells using Al-clad SS-316 positive cans and various separators, including Celgard K1640, Celgard 2325, Celgard 2500, Celgard 3501, and PVDF-coated Celgard 2500.

2325 separator, which is a PP/PE/PP trilayer, performed much better than the cells with a Celgard 2500 PP separator. This finding indicates that incorporating stable PE into a PP membrane can significantly improve the performance of PP against oxidation at high voltages, and especially the high-rate capability; although, the cell with a PP/PE/PP separator still exhibits lower capacity than a cell with the PE separator. The performance of the cells with Celgard 2500 PP membrane can be improved further by coating with a thin layer of PVDF on the membrane surface. The cell with a PVDF-coated Celgard 2500 separator exhibited a slightly lower capacity than a cell with the Celgard K1640 separator but slightly higher capacity than a cell with the Celgard 2325 separator. Cells with these three separators show nearly the same high-rate performances at a 5C rate.

Regarding long-term cycling stability, cells with Celgard K1640 and PVDF-coated Celgard 2500 separators have the highest cycling stability, with only 0.01% capacity fading per cycle after the rate performance test for both separators. The cell with a Celgard 2325 separator exhibits a slightly lower, but still good, stability of 0.02% capacity fading per cycle after the rate performance test. However, cells with Celgard 2500 and Celgard 3501 separators exhibited poor cycling stability after rate performance tests (0.05% and 0.07% capacity fading per cycle, respectively).

To further investigate the fundamental mechanism that affects the performance of the cells with different separators, the surface conditions of these separators before and after cycling were analyzed by XPS, and the results are compared in Fig. 7. As for the fresh separators before cycling (shown as the bottom curves in each figure box), the uncoated separators (Celgard K1640, 2325, and 2500) have only a carbon (C) element, indicating a pure polyolefin structure. Celgard 3501 shows extra peaks for silicon and oxygen, which indicate some of the components of the surfactant used for the coating. The PVDF-coated Celgard 2500 separator shows high-intensity F and reduced C, which is consistent with the ratio of C/F in PVDF. After cycling, the XPS spectra of all the separators, except for the Celgard K1640 PE separator, show a significant increase in the peak intensity of O. More importantly, new peaks corresponding to Li, P, and F also are found in these spectra of the cycled separators, which are additional strong evidence that the reactions occur between the separators and electrolyte components during cycling, especially during the charging process.

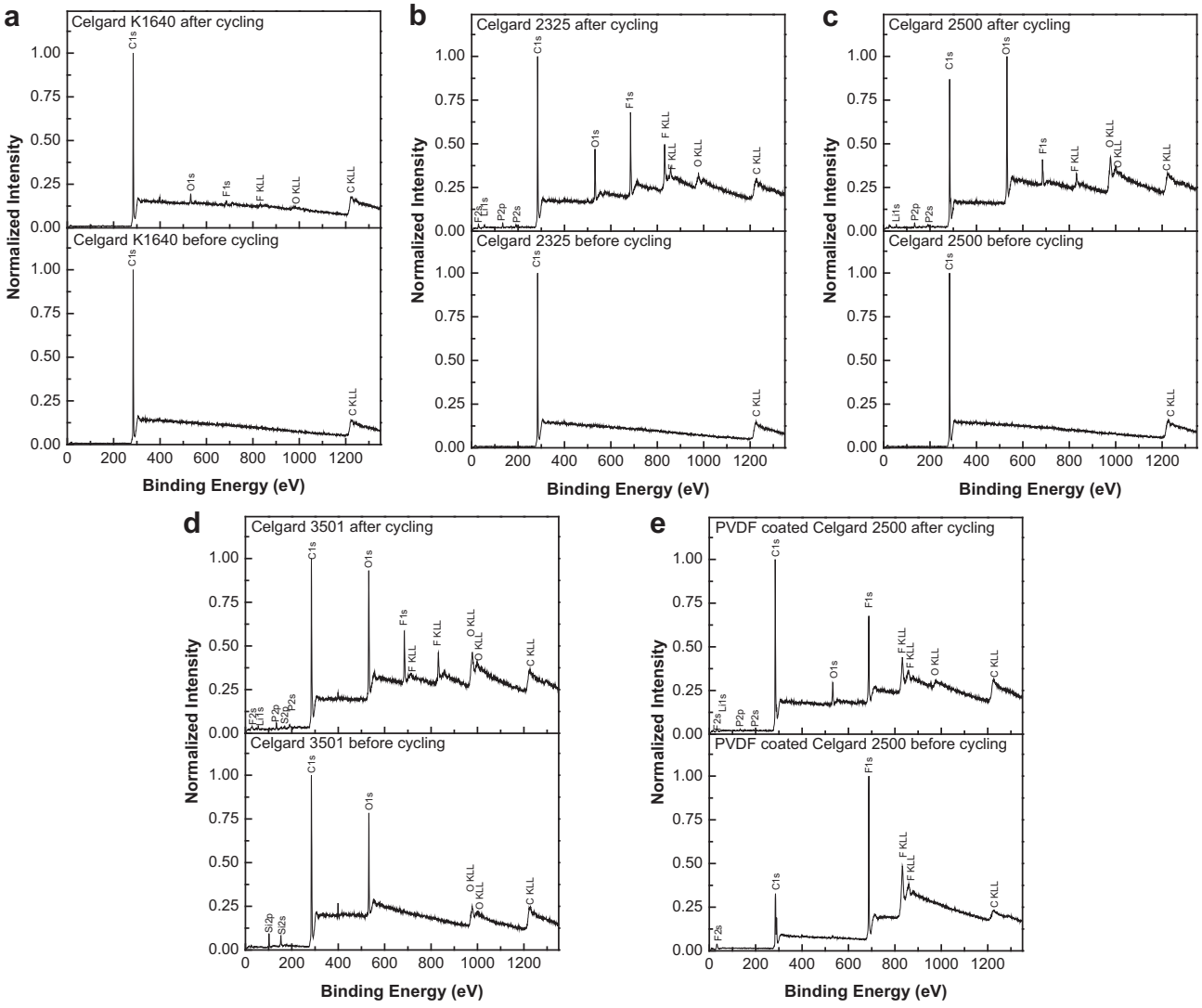

Fig. 7. XPS spectra of a) Celgard K1640, b) Celgard 2325, c) Celgard 2500, d) Celgard 3501, and e) PVDF-coated Celgard 2500 separators before and after cycling in Li/$LiCr_{0.05}Ni_{0.45}Mn_{1.5}O_4$ half cells using Al-clad SS-316 coin cell cans.

For the cycled Celgard 1640 PE separator, the intensities of the new XPS peaks for O and F between 300 and 1200 eV are much smaller than those observed in other cycled separators. This finding is consistent with the CV and cell performance results shown in Figs. 5 and 6 in which cells using the Celgard K1640 PE separator demonstrate the most stable electrochemical behavior. The results discussed above indicate that the surface reactions between the electrolyte and the separators produce deposits on the surface of the separators, especially on PP/PE/PP, PP, and surfactant-coated PP (see Fig. 7(b)–(d)). These deposits will increase the cell impedance and lead to poor rate capability (see Fig. 6). On the other hand, a small amount of reaction product is observed on the cycled PVDF-coated PP and PE separators (see Fig. 7(a) and (e)), which means that the PVDF and PE surfaces are stable to the non-aqueous electrolyte (1M $LiPF_6$ in EC/EMC (3:7 in volume)) at voltages as high as 4.9 V vs. Li/Li^+ used in this work. Among the various separators investigated in this work, the PE separator is the best candidate for use in high-voltage Li-ion batteries.

FTIR was used to further study the oxidation products on the separators and the results are compared in Fig. 8. Celgard K1640 and Celgard 2325 separators show identical FTIR spectra before and after cycling (Fig. 8(a) and (b)), which corroborates the above XPS results. Compared to the fresh separators before cycling (shown as the bottom curves in each figure box), Celgard 2500 and PVDF-coated Celgard 2500 separators after cycling have three new peaks (indicated by arrows in Fig. 8(c) and (e)), characteristic for P═O stretching at 1275 cm^{-1} and P–O bending at 940 cm^{-1} and 750 cm^{-1} [24,25]. The new bonds of P═O and P–O existing at the surface of these two separators clearly indicate the reactions of the separators and the electrolyte at the surface of the cathode and at high voltages because the phosphorus element only exists in electrolyte solute $LiPF_6$. This result is also consistent with the XPS results that show new elements (F and P) on the surfaces of separators, where the new elements are from the reactions among separators, electrolyte components and active electrode materials, but not from the electrolyte adsorption because all tested separator samples were thoroughly washed with EMC and dried. SEM images in Fig. 9 shows that PVDF coating does not completely cover the Celgard 2500 surface therefore phosphorus element, solely from $LiPF_6$ solute, is detected by FTIR in both cases. However, the main disadvantage of PP-based separator is that PP itself is easily oxidized at high voltages (as will be discussed in the following

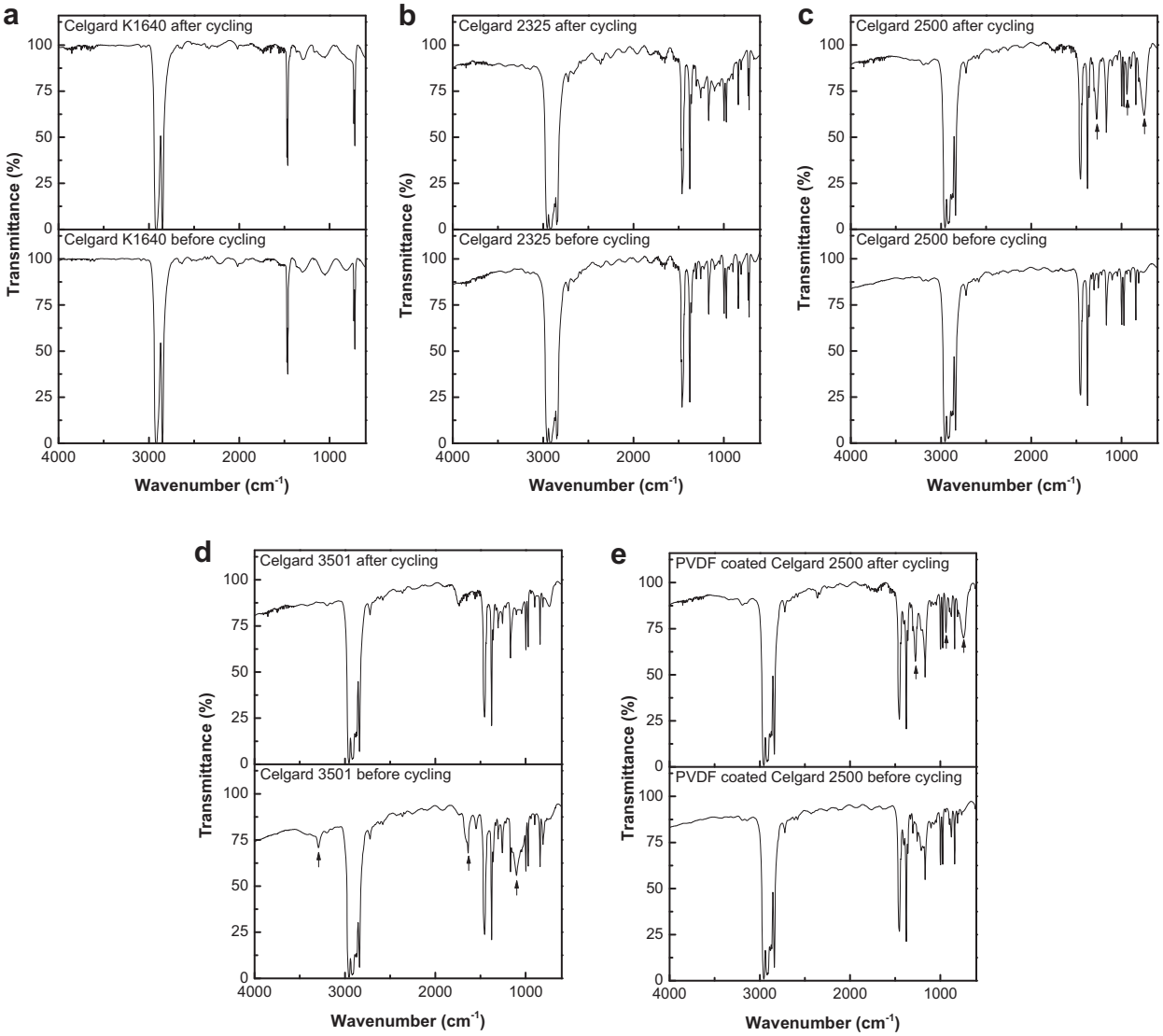

Fig. 8. FTIR spectra of a) Celgard K1640, b) Celgard 2325, c) Celgard 2500, d) Celgard 3501, and e) PVDF-coated Celgard 2500 separators before and after cycling in $Li/LiCr_{0.05}Ni_{0.45}Mn_{1.5}O_4$ half cells using Al-clad SS-316 coin cell cans.

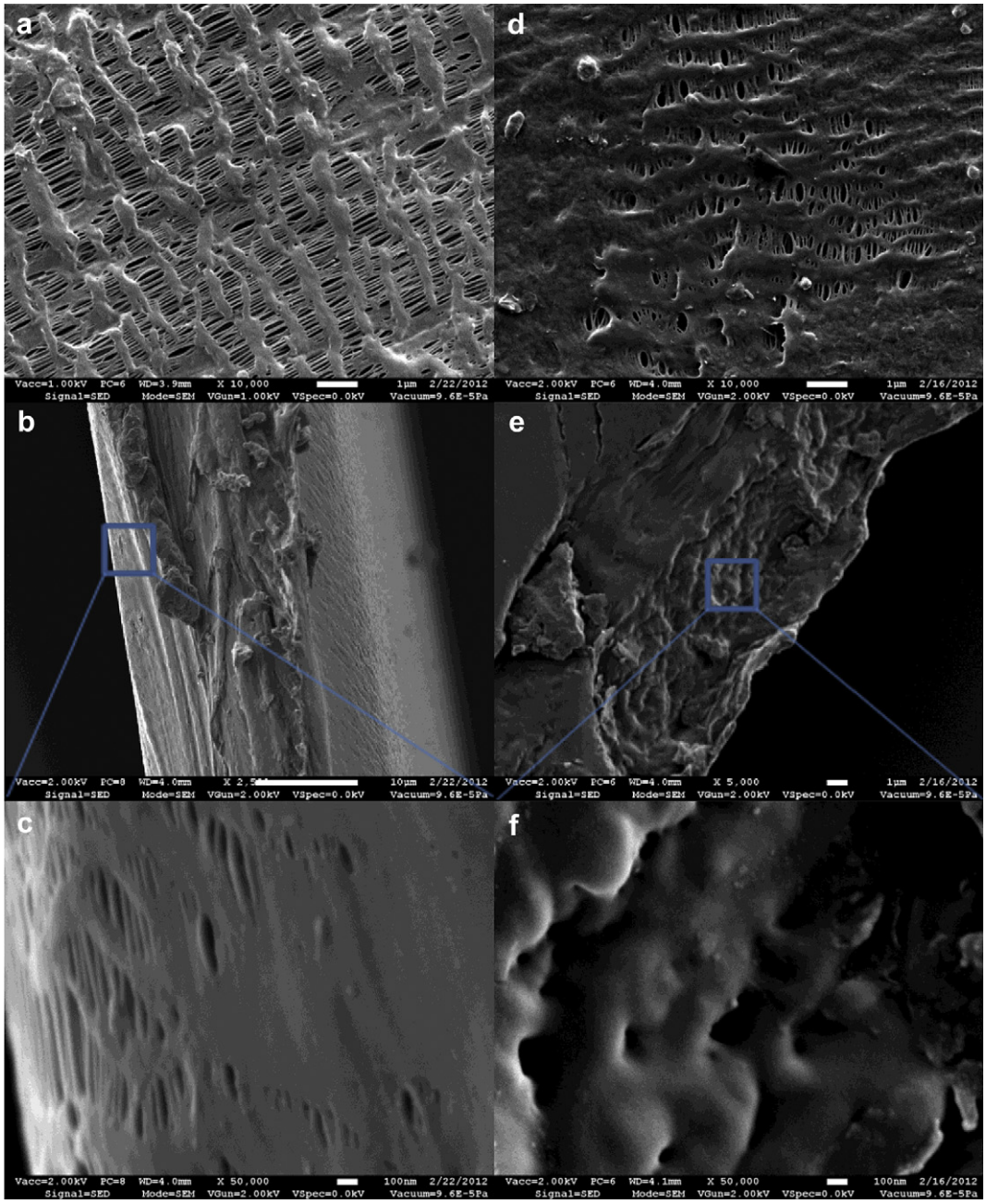

Fig. 9. SEM images of (a) Surface and (b, c) cross-section of Celgard 2500 and (d) Surface and (e, f) cross-section of PVDF-coated Celgard 2500.

section about simulated calculations about HOMO energies of PE, PP and PVDF) and reacts with the electrolyte components such as carbonate solvents and $LiPF_6$ salt leading to the increased impedance of the cell. After coating PVDF on Celgard 2500, although not fully covered, direct contact between PP and $LiPF_6$/carbonate is largely reduced, and thus greatly improved electrochemical behaviors are observed.

As demonstrated by the XPS result, silicon element exists in the surface coating of Celgard 3501 separator. In FTIR spectrum, characteristic peaks of Si–O–H stretching at 3292 cm^{-1}, Si–O–C bending at 1638 cm^{-1} and Si–O–Si stretching at 1101 cm^{-1} [26–29] are also found for fresh separator (as indicated by arrows in the bottom curve of Fig. 8(d)). After cycling, these peaks related to the silicon compound as surfactant on Celgard 3501 separator disappear. The loss of these peaks means the surfactant on Celgard 3501 is not stable with the electrolyte and active electrode materials at high voltages. The poor stability of the surfactant on Celgard 3501 results in the significantly low initial efficiency of cells using Celgard 3501 as the separator.

Since the basic materials in the above five separators are PP, PE and PVDF, to further understand the electrochemical stability difference of PE, PP and PVDF separators, the HOMO and LUMO energies of the model polymers (PE, PP, and PVDF) materials were calculated using DFT method. All calculations were performed using Gaussian 09 program [30] at the B3LYP/6-31G* (d,p) level. Because previous DFT calculations indicated that the calculations of HOMO and LUMO energy levels for PE and PP were weakly dependent on the basis set used or the actual geometry (isolated chain or bulk polyethylene) [31,32], the PE, PP, and PVDF polymers were modeled using one-dimensional chain molecules in this work, i.e., $CH_3(CH_2)_6CH_3$,

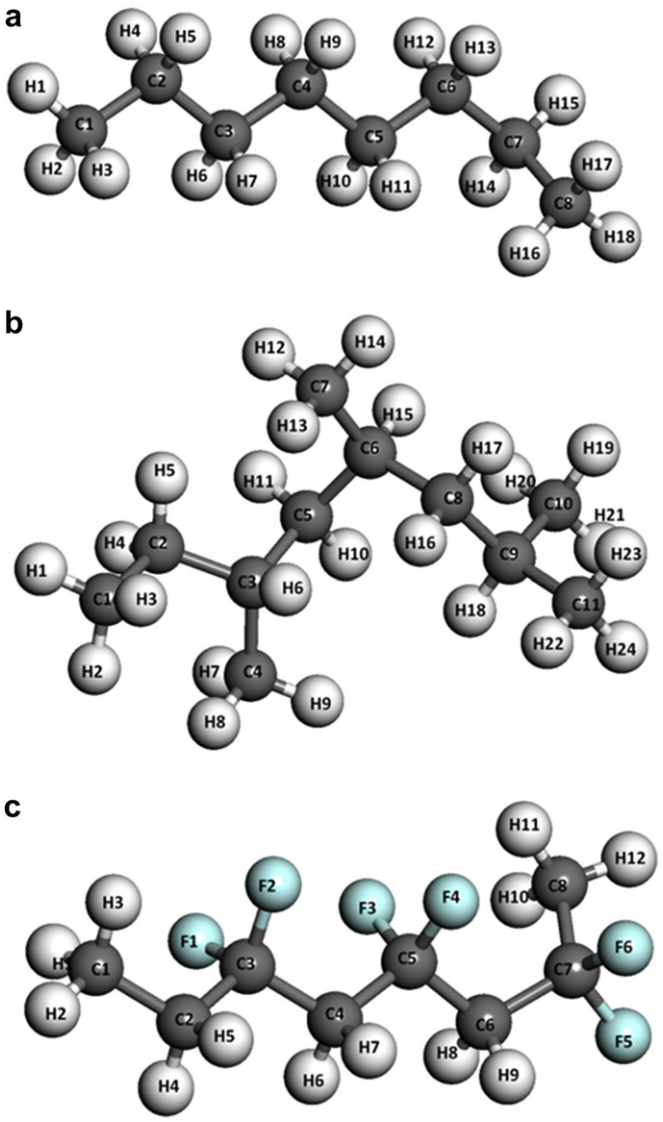

Fig. 10. The optimized geometries of model PE (a), PP (b) and PVDF (c) molecules.

$CH_3[CH(CH_3)CH_2]_3CH_3$ and $CH_3(CF_2CH_2)_3CH_3$. Fig. 10 shows the optimized structures, Table 1 lists the calculated HOMO and LUMO energies and LUMO–HOMO energy gaps, and Table 2 lists the Mulliken atomic charges of each atom on each model molecule for PE, PP and PVDF. These eigenvalues of LUMO and HOMO energies and their energy gaps reflect the chemical activity and oxidation potentials of the materials. HOMO as an electron donor represents the ability to donate an electron while LUMO as an electron acceptor represents the ability to obtain an electron. The smaller the LUMO and HOMO energy gaps, the easier it is for the HOMO electrons to be excited; the higher the HOMO energies, the easier it is for HOMO to donate electrons (being oxidized); the lower the LUMO energies, the easier it is for LUMO to accept electrons (being reduced). As shown in Table 1, the HOMO energy of PP is higher than those of PE and PVDF, suggesting that both PE and PVDF are electrochemically more stable (against oxidation) than PP. This is consistent with our experimental observation. On the other hand, as shown in Table 2, the absolute values of the calculated Mulliken charges of C atoms of the CH groups in PP molecule are in the range of 0.03 ~ 0.07 |e|, which are smaller than the corresponding charges in absolute values (0.15 ~ 0.61 |e|) of C atoms in CH_2, CH_3 and CF_2 groups. One can assume that the lower absolute value of the Mulliken atomic charge means the higher possibility of being further oxidized [33]. Therefore, the higher electrochemical activity of the CH group in PP might be the possible cause for lower oxidation-resistant stability of the PP material.

Table 1
The calculated HOMO, LUMO energies and LUMO–HOMO gaps for PE, PP and PVDF.

Molecule	E_{HOMO} (eV)	E_{LUMO} (eV)	$E_{LUMO-HOMO\ gap}$ (eV)
PE	−8.07	2.46	10.53
PP	−6.91	1.98	8.89
PVDF	−8.49	1.64	10.13

Table 2
DFT calculated Mulliken charges (in |e|) of each atom in PE, PP and PVDF.

PE		PP		PVDF	
Atom	Charge	Atom	Charge	Atom	Charge
C1	−0.316	C1	−0.323	C1	−0.332
H1	0.105	H1	0.104	H1	0.107
H2	0.099	H2	0.100	H2	0.126
H3	0.100	H3	0.099	H3	0.127
C2	−0.176	C2	−0.172	C2	−0.227
H4	0.090	H4	0.094	H4	0.108
H5	0.089	H5	0.087	H5	0.112
C3	−0.170	C3	−0.036	C3	0.618
H6	0.086	H6	0.082	F1	−0.307
H7	0.086	C4	−0.324	F2	−0.303
C4	−0.171	H7	0.098	C4	−0.290
H8	0.091	H8	0.099	H6	0.132
H9	0.086	H9	0.100	H7	0.128
C5	−0.174	C5	−0.180	C5	0.615
H10	0.087	H10	0.083	F3	−0.304
H11	0.087	H11	0.087	F4	−0.297
C6	−0.166	C6	−0.067	C6	−0.295
H12	0.087	H12	0.083	H8	0.132
H13	0.087	C7	−0.314	H9	0.133
C7	−0.173	H13	0.103	C7	0.599
H14	0.091	H14	0.095	F5	−0.314
H15	0.091	H15	0.096	F6	−0.298
C8	−0.317	C8	−0.148	C8	−0.362
H16	0.101	H16	0.082	H10	0.121
H17	0.101	H17	0.080	H11	0.129
H18	0.099	C9	−0.063	H12	0.142
		H18	0.088		
		C10	−0.310		
		H19	0.096		
		H20	0.098		
		H21	0.097		
		C11	−0.310		
		H22	0.098		
		H23	0.102		
		H24	0.096		

4. Conclusions

The results from our systematic investigations of the inactive materials in batteries (including coin cell positive cans and separators) indicates that every component used in conventional Li-ion batteries have to be re-examined when high voltage (i.e., >4.5 V) cathodes such as $LiNi_{0.5}Mn_{1.5}O_4$ are used. For such high-voltage batteries, the batteries with Al-clad SS-316 positive cans exhibit much better electrochemical stability than batteries with the bare SS-316 positive cans, which exhibit additional anodic oxidations. The improved stability is mainly due to the thin, but dense, alumina protective layer on the surface of the Al-clad positive can that is stable against oxidation at high voltages. A further investigation of the electrochemical stability of separators indicates that PE-based separator (such as Celgard K1640) is the most stable separator among five different separators investigated for high-voltage spinel

cathode materials. The surface reactions occurring among the active material, the separator and the electrolyte at high voltages may lead to undesired deposits on the surface of the separators. Such surface deposits are detrimental to the first-cycle efficiency, capacity, rate capability, and long-term cycling stability of high-voltage Li-ion batteries. To study high voltage cathode materials, a stable separator should be used to avoid the side reactions which may have detrimental effects on the electrochemical performance of the testing cells.

Acknowledgments

This work was supported by the Assistant Secretary for Energy Efficiency and Renewable Energy, Office of Vehicle Technologies of the U.S. Department of Energy under Contract No. DE-AC02-05CH11231, Subcontract No 18769 under the Batteries for Advanced Transportation Technologies (BATT) Program. The XPS measurements were performed in the Environmental Molecular Sciences Laboratory, a national scientific user facility sponsored by the DOE's Office of Biological and Environmental Research and located at Pacific Northwest National Laboratory. Mr. Paul A. Peterson and Mr. Fred Humiston of Celgard, LLC are gratefully acknowledged for supplying the Celgard separators for this study. The authors thank Dr. Kang Xu at the U.S. Army Research Laboratory for useful discussions.

References

[1] J.B. Goodenough, Y. Kim, Chem. Mater. Rev. 22 (2010) 587.
[2] M.S. Whittingham, Chem. Rev. 104 (2004) 4271.
[3] P.G. Bruce, B. Scrosati, J.-M. Tarascon, Angew. Chem. Int. Ed. 47 (2008) 2930.
[4] O.K. Park, Y. Cho, S. Lee, H.-C. Yoo, H.-K. Song, J. Cho, Energy Environ. Sci 4 (2011) 1621.
[5] R. Santhanam, B. Rambabu, J. Power Sources 195 (2010) 5442.
[6] K.M. Shaju, P.G. Bruce, Dalton Trans. (2008) 5471.
[7] T.A. Arunkumar, A. Manthiram, Electrochim. Acta 50 (2005) 5568.
[8] G.Q. Liu, W.S. Yuan, G.Y. Liu, Y.W. Tian, J. Alloys Compd. 484 (2009) 567.
[9] Y.-K. Sun, K.-J. Hong, J. Prakash, K. Amine, Electrochem. Commun. 4 (2002) 344.
[10] D.W. Shin, A. Manthiram, Electrochem. Commun. 13 (2011) 1213.
[11] S.-T. Myung, K.-S. Lee, D.-W. Kim, B. Scrosati, Y.-K. Sun, Energy Environ. Sci 4 (2011) 935.
[12] G.B. Zhong, Y.Y. Wang, Z.C. Zhang, C.H. Chen, Electrochim. Acta 56 (2011) 6554.
[13] X. Zhang, H. Zheng, V. Battaglia, R.L. Axelbaum, Proc. Combust. Inst. 33 (2011) 1867.
[14] D. Wang, J. Xiao, W. Xu, Z. Nie, C. Wang, G.L. Graff, J.-G. Zhang, J. Power Sources 196 (2011) 2241.
[15] J. Xiao, X. Chen, P.V. Sushko, M.L. Sushko, L. Kovarik, J. Feng, Z. Deng, J. Zheng, G.L. Graff, Z. Nie, D. Choi, J. Liu, J.-G. Zhang, M.S. Whittingham, Adv. Mater. 24 (2012) 2109.
[16] N.N. Sinha, J.C. Burns, R.J. Sanderson, J. Dahn, J. Electrochem. Soc 158 (2011) A1400.
[17] M. Kunduraci, J.F. Al-Sharab, G.G. Amatucci, Chem. Mater. 18 (2006) 3585.
[18] J.-H. Kim, S.-T. Myung, C.S. Yoon, S.G. Kang, Y.-K. Sun, Chem. Mater. 16 (2004) 906.
[19] K. Ariyoshi, Y. Iwakoshi, N. Nakayama, T. Ohzuku, J. Electrochem. Soc 151 (2004) A296.
[20] K. Takahashi, M. Saitoh, M. Sano, M. Fujita, K. Kifune, J. Electrochem. Soc 151 (2004) A173.
[21] M. Kunduraci, G.G. Amatucci, J. Electrochem. Soc 153 (2006) A1345.
[22] J.H. Kim, C.S. Yoon, S.T. Myung, J. Prakash, Y.K. Sun, Electrochem. Solid-State Lett. 7 (2004) A216.
[23] S. Patoux, L. Sannier, H. Lignier, Y. Reynier, C. Bourbon, S. Jouanneau, F.L. Cras, S. Martinet, Electrochim. Acta 53 (2008) 4137.
[24] K. Rajendran, C.D. Keefe, Cryst. Res. Technol. 45 (2010) 939.
[25] P.Y. Shih, S.W. Yung, T.S. Chin, J. Non-Cryst. Solids 244 (1999) 211.
[26] A. Beganskiene, V. Sirutkaitis, M. Kurtinaitiene, R. Juskenas, A. Karerva, Mater. Sci. 10 (2004) 287.
[27] J. Serra, P. Gonzalez, S. Liste, C. Serra, S. Chiussi, B. Leon, M. Perez-Amor, H.O. Ylanen, M. Hupa, J. Non-Cryst. Solids 332 (2003) 20.
[28] H. Yoshida, S. Narisawa, S. Fujita, R. Liu, M. Arai, Phys. Chem. Chem. Phys. 14 (2012) 4727.
[29] G.E.A. Swann, S.V. Patwardhan, Clim. Past 7 (2011) 65.
[30] R.A. Gaussian 09, M.J. Frisch, G.W. Trucks, H.B. Schlegel, G.E. Scuseria, M.A. Robb, J.R. Cheeseman, G. Scalmani, V. Barone, B. Mennucci, G.A. Petersson, H. Nakatsuji, M. Caricato, X. Li, H.P. Hratchian, A.F. Izmaylov, J. Bloino, G. Zheng, J.L. Sonnenberg, M. Hada, M. Ehara, K. Toyota, R. Fukuda, J. Hasegawa, M. Ishida, T. Nakajima, Y. Honda, O. Kitao, H. Nakai, T. Vreven, Jr., J.A. Montgomery, J.E. Peralta, F. Ogliaro, M. Bearpark, J.J. Heyd, E. Brothers, K.N. Kudin, V.N. Staroverov, R. Kobayashi, J. Normand, K. Raghavachari, A. Rendell, J.C. Burant, S. S. Iyengar, J. Tomasi, M. Cossi, N. Rega, N.J. Millam, M. Klene, J.E. Knox, J.B. Cross, V. Bakken, C. Adamo, J. Jaramillo, R. Gomperts, R.E. Stratmann, O. Yazyev, A.J. Austin, R. Cammi, C. Pomelli, J.W. Ochterski, R.L. Martin, K. Morokuma, V.G. Zakrzewski, G.A. Voth, P. Salvador, J.J. Dannenberg, S. Dapprich, A.D. Daniels, Ö. Farkas, J.B. Foresman, J.V. Ortiz, J. Cioslowski, D.J. Fox, Gaussian, Inc., Wallingford CT, 2009.
[31] F. Picaud, A. Smogunov, A. Dal Corso, E. Tosatti, J. Phys. Cond. Matter 15 (2003) 3731.
[32] P. Cysewski, A. Shyichuk, Macromol. Theory Simul 15 (2006) 331.
[33] J. Barbee, A.E. Kuznetsov, Comp. Theor. Chem. 981 (2012) 73.